

# Unsupervised Monocular Depth Estimation with Left-Right Consistency

Clément Godard, Oisin Mac Aodha, and Gabriel J. Brostow  
<http://visual.cs.ucl.ac.uk/pubs/monoDepth>

**Abstract**—Learning based methods have shown very promising results for the task of depth estimation in single images. However, most existing approaches treat depth prediction as a supervised regression problem and as a result, require vast quantities of corresponding ground truth depth data for training. Just recording quality depth data in a range of environments is a challenging problem. In this paper, we innovate beyond existing approaches, replacing the use of explicit depth data during training with easier-to-obtain binocular stereo footage.

We propose a novel training objective that enables our convolutional neural network to learn to perform single image depth estimation, despite the absence of ground truth depth data. By exploiting epipolar geometry constraints, we generate disparity images by training our networks with an image reconstruction loss. We show that solving for image reconstruction alone results in poor quality depth images. To overcome this problem, we propose a novel training loss that enforces consistency between the disparities produced relative to both the left and right images, leading to improved performance and robustness compared to existing approaches. Our method produces state of the art results for monocular depth estimation on the KITTI driving dataset, even outperforming supervised methods that have been trained with ground truth depth.

**Index Terms**—Monocular depth estimation, stereo, depth CNNs, 2D-to-3D

## 1 INTRODUCTION

Depth estimation from images has a long history in computer vision. Fruitful approaches have relied on structure from motion, shape from X, binocular, and multi-view stereo. However, most of these techniques rely on the assumption that multiple observations of the scene of interest are available. These observations can come in the form of multiple viewpoints, or observations of the scene under different lighting conditions. To overcome this limitation, there has recently been a surge in the number of works that pose the task of monocular depth estimation as a supervised learning problem [1], [2], [3]. These methods attempt to directly predict the depth of each pixel in an image using models that have been trained offline on large collections of ground truth depth data. While these methods have enjoyed great success, to date they have been restricted to scenes where large image collections and their corresponding pixel depths are available.

Understanding the shape of a scene from a single image, independent of its appearance, is a fundamental problem in machine perception. There are many applications such as synthetic object insertion in computer graphics [4], synthetic depth of field in computational photography [5], grasping in robotics [6], using depth as a cue in human body pose estimation [7], robot assisted surgery [8], and automatic 2D to 3D conversion in film [9]. Accurate depth from one or more cameras is also crucial for self driving cars, where expensive laser based systems are often used.

Humans perform well at monocular depth estimation by exploiting cues such as perspective, scaling relative to the known size of familiar objects, appearance in the form of lighting and shading, occlusion, among other cues [10]. This combination of both top-down and bottom-up cues appears to link full scene

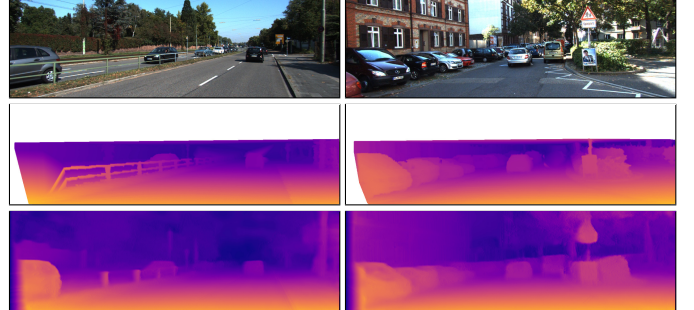


Fig. 1. Results from our method on KITTI 2015. Top to bottom: Input left image, ground truth disparities, and our result. Our method is able to capture fine details in the image, such as streets signs and poles.

understanding with our ability to accurately estimate depth. In this work, we take an alternative approach and treat automatic depth estimation as an image reconstruction problem during training. Our fully convolutional model does not require any depth data, and is instead trained to synthesize depth as an intermediate. It learns to predict the pixel level correspondence between pairs of rectified stereo images that have a known camera baseline. Concurrently to this work, there are some existing methods that also address the same problem. But those have several limitations e.g. they are not fully differentiable, making training suboptimal [11], or they have image formation models that do not scale to large output resolutions [9]. We improve upon these methods with a novel training objective and enhanced network architecture, to significantly increase the quality of our final results.

An example result from our algorithm is illustrated in Fig. 1. Our method is fast and only takes on the order of 50 milliseconds to predict dense depth for a  $768 \times 256$  image on a modern GPU. Specifically, we propose the following contributions:

• Clément Godard, Oisin Mac Aodha, and Gabriel J. Brostow are with the Department of Computer Science, University College London.

Manuscript received XXX; revised XXX.

- 1) A network architecture that performs end-to-end unsupervised monocular depth estimation with a novel training loss that incorporates a left-right depth consistency constraint inside the network.
- 2) An evaluation of several different training losses and image formation models highlighting the effectiveness of our approach.
- 3) In addition to showing state of the art results on a challenging driving dataset, we also show that our model generalizes to three other different datasets, including a new outdoor urban dataset that we have collected ourselves.

## 2 RELATED WORK

There is a large body of work that focuses on depth estimation from images, either using pairs [12], several overlapping images captured from different viewpoints [13], temporal sequences [14], or assuming a fixed camera, static scene, and changing lighting [15], [16]. These approaches are typically only applicable when there is more than one input image available of the scene of interest. Here we focus on works related to monocular depth estimation, where there is only a single input image, and no assumptions about the scene geometry or types of objects present are made.

### Learning Based Stereo

The vast majority of stereo estimation algorithms have a data term which computes the similarity between each pixel in the first image and every other pixel in the second image. Typically the stereo pair is rectified and thus the problem of disparity (i.e. scaled inverse depth) estimation can be posed as a 1D search problem for each pixel. Recently, it has been shown that instead of using hand defined similarity measures, treating the matching as a supervised learning problem and training a function to predict the correspondences produces far superior results [17], [18]. It has also been shown that posing this binocular correspondence search as a multi-class classification problem has advantages both in terms of quality of results and speed [19].

Instead of just learning the matching function, Mayer et al. [20] introduced a fully convolutional [21] deep network called DispNet that directly computes the correspondence field between two images. At training time, they attempt to directly predict the disparity for each pixel by minimizing a regression training loss. DispNet has a similar architecture to their previous end-to-end deep optical flow network [22].

The above methods rely on having large amounts of accurate ground truth disparity data and stereo image pairs at training time. This type of data can be difficult to obtain for real world scenes, so these approaches typically use synthetic data for training. Synthetic data is becoming more realistic, e.g. [23], but still requires the manual creation of new content for every different application scenario.

### Supervised Single Image Depth Estimation

Single view, or monocular, depth estimation refers to the problem setup where only a single image is available at test time.

Saxena et al. [24] proposed a patch based model known as Make3D that first over-segments the input image into patches and then estimates the 3D location and orientation for local planes to explain each patch. The predictions of the plane parameters are made using a linear model trained offline on a dataset of laser scans, and the predictions are then combined together using an

MRF. The disadvantage of this method, and other planar based approximations, e.g. [25], is that they can have difficulty modeling thin structures and, as predictions are made locally, lack the global context required to generate realistic outputs. Instead of hand-tuning the unary and pairwise terms, Liu et al. [3] use a convolutional neural network (CNN) to learn them. In another local approach, Ladicky et al. [1] incorporate semantics into their model to improve their per pixel depth estimation.

Karsch et al. [26] attempt to produce more consistent image level predictions. Their approach transfers depths from the most suitable depth image training candidates, at a whole image level, by performing a lookup. A drawback of this approach is that it relies on the entire dataset being available at test time.

Eigen et al. [2], [27] showed that it was possible to produce dense pixel depth estimates using a two scale deep network, trained on images and their corresponding depth values. Unlike other previous work in single image depth estimation, they do not rely on hand crafted features or an initial over-segmentation and instead learn a representation directly from the raw pixel values. Several works have built upon the success of this approach using techniques such as CRFs to improve the detail [28], changing the loss from a regression one to classification [29], using other more robust loss functions [30], and by incorporating strong scene priors in the case of the related problem of surface normal estimation [31].

Again, like the previous stereo methods, these approaches rely on having high quality, pixel aligned, ground truth depth at training time. We too perform single depth image estimation, but train with an added binocular color image, instead of requiring ground truth depth.

### Unsupervised Depth Estimation

Recently, a small number of deep network based methods for novel view synthesis and depth estimation have been proposed, which do not require ground truth depth at training time.

Flynn et al. [32] introduced a novel image synthesis network called DeepStereo that generates new views by selecting pixels from nearby neighboring images. During training, they choose a set of images, compute their respective camera poses (using a combination of odometry and standard structure from motion), and then train a network to predict the appearance of a held out nearby image: the most appropriate depths are selected to sample colors from the neighboring images, based on plane sweep volumes. At test time, image synthesis is performed on small overlapping patches. However, DeepStereo is not suitable for monocular depth estimation as it requires several nearby posed images at test time.

The Deep3D network of Xie et al. [9] also addresses the problem of novel view synthesis, where their goal is to generate the corresponding right view from an input left image (i.e. the source image) in the context of binocular pairs. Again using an image reconstruction loss, their method produces a distribution over all the possible disparities for each pixel. The resulting synthesized right image pixel values are a combination of the pixels on the same scan line from the left image, weighted by the probability of each disparity. The disadvantage of their image formation model is that increasing the number of candidate disparity values greatly increases the memory consumption of the algorithm, making it difficult to scale their approach to bigger output resolutions. In this work, we perform a comparison to the Deep3D image formation model, and show that our algorithm produces superior results.

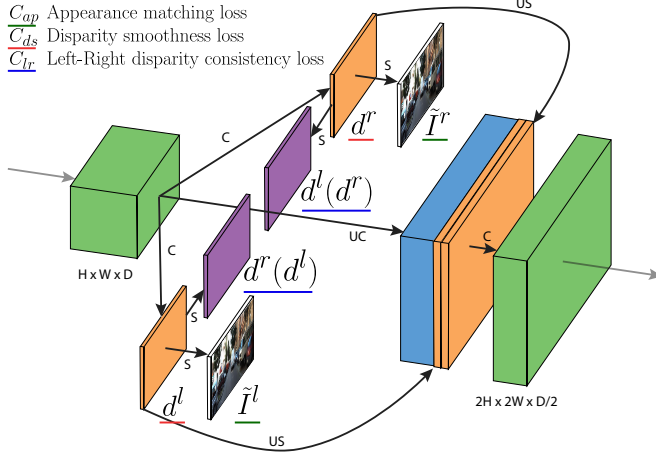


Fig. 2. Our loss module outputs disparity maps,  $d^l$  and  $d^r$ , from both the left and right images. The loss computation combines smoothness, reconstruction, and left-right disparity-consistency terms. This same module is repeated at each of the four different output scales. C: Convolution, UC: Up-Convolution, S: Bilinear Sampling, US: Up-Sampling.

Closest to our model in spirit is the concurrent work of Garg et al. [11]. Like Deep3D and our method, they train a network for monocular depth estimation using an image reconstruction loss. However, their image formation model is not fully differentiable. To compensate, they perform a Taylor approximation to linearize their loss resulting in an objective that is more challenging to optimize. Similar to other recent work, e.g. [33], [34], [35], our model overcomes this problem by using bilinear interpolation when sampling from the source image [36], resulting in a fully differentiable training loss.

In this work, we propose a fully convolutional deep neural network loosely inspired by the supervised DispNet architecture of Mayer et al. [20]. By posing monocular depth estimation as an image reconstruction problem during training, we can solve for the disparity field without requiring ground truth depth anywhere in the process. However, only minimizing a photometric loss can result in good quality image reconstructions but poor quality depth. Among other terms, our fully differentiable training loss includes a left-right consistency check to improve the quality of our synthesized depth images. This type of consistency check is commonly used as a post processing step in many stereo methods, e.g. [17], but we incorporate it directly during training in our network.

### 3 METHOD

This section describes our single image depth prediction network. We introduce a novel depth estimation training loss, featuring an inbuilt consistency check, which enables us to train on image pairs without requiring supervision in the form of ground truth depth.

#### 3.1 Depth Estimation as Image Reconstruction

Given a single image  $I$  at test time, our goal is to learn a function that can predict the per-pixel scene depth,  $\hat{d} = f(I)$ . Most existing learning based approaches treat this as a supervised learning problem, where for training, each color input image is somehow supplied with its intended output, the corresponding depth. It is presently not practical to acquire this ground truth depth data for a large variety of scenes. Even expensive hardware, such as laser

scanners, can be imprecise in natural scenes, featuring movement and reflections. As an alternative, we instead pose depth estimation as an image reconstruction problem during training. The intuition here is that given a calibrated pair of binocular cameras, if we can learn a function that is able to reconstruct one image given the other, then we have learned something about the shape of the scene that is being imaged.

Specifically, at training time, we have access to two images  $I^l$  and  $I^r$ , corresponding to the left and right color images from a calibrated stereo pair, captured at the same moment in time. Instead of trying to directly predict the depth, we instead attempt to find the correspondence field  $d^r$  that when applied to the left image would enable us to reconstruct the right image,  $\arg \min_{d^r} \|I^r - I^l(d^r)\|$ . We will refer to the reconstructed image  $I^l(d^r)$  as  $I^r$ . Similarly, we can also estimate the left image given the right one,  $\tilde{I}^l = I^r(d^l)$ . Assuming that the images are rectified [37],  $d$  corresponds to the image disparity - a scalar value per pixel that our model will learn how to predict. Given the baseline distance,  $b$ , between the cameras and the camera focal length,  $f$ , we can then trivially recover the depth from the predicted disparity,  $\hat{d} = b f / d$ .

#### 3.2 Depth Estimation Network

The key insight of our method is that we can produce superior depth maps by predicting the disparity from both binocular cameras, and enforcing them to be consistent with each other. Generating the right view with pixels from the left view leads to a disparity map aligned with the right view (and vice versa). As we would like the disparity map to be aligned to the input image, which we fix as the left view, we train our network to estimate both disparity maps. During training we have access to both the left and right stereo images. While only the left view is fed through the network during both training and testing, at training time we can still sample pixels from the right view when generating a left view prediction. Our goal is to reconstruct the corresponding left and right views by learning the disparity maps that can shift the pixels to minimize the image reconstruction error.

Our fully convolutional architecture is inspired by DispNet [20], but features several important modifications that enable us to train without requiring ground truth depth. The structure of our network is illustrated in Table 1. The network is composed of two main parts - an encoder (from conv1 to conv7b) and decoder (from upconv7). The decoder uses skip connections [21] from the encoder's activation blocks, which enable it to resolve higher resolution details. We output disparity predictions at four different scales (disp4 to disp1), which increase in spatial resolution at each of the subsequent scales. When training the network, two disparity maps are predicted at each of the output scales, one aligned with the input to the network and the other aligned to its corresponding stereo partner.

#### 3.3 Training Loss

Our loss function at each output scale,  $s$ , is composed of a weighted combination of three main terms,

$$C_s = \alpha_{ap}(C_{ap}^l + C_{ap}^r) + \alpha_{ds}(C_{ds}^l + C_{ds}^r) + \alpha_{lr}(C_{lr}^l + C_{lr}^r), \quad (1)$$

where  $C_{ap}$  encourages the reconstructed image to be similar to the corresponding training input,  $C_{ds}$  enforces smooth disparities, and  $C_{lr}$  attempts to make the predicted disparities from the left and right images consistent. Each of the main terms contains both

a left and right image variant. The left image is obviously always passed through the network. Since we have access to the right view during training, we can also predict a disparity map in its frame of reference. We illustrate our loss module in Fig. 2. The final total loss is a weighted sum of the individual scaled losses,

$$C = \sum_{s=1}^4 \lambda_s C_s, \quad (2)$$

where  $\lambda_s$  allows us to weight the relative importance of different output scales during training.

In the following explanation, we present the individual components of our loss in terms of the left image (e.g.  $C_{ap}^l$ ). The right image versions, e.g.  $C_{ap}^r$ , just require one to sample in the opposite direction.

### Appearance Matching Loss

During training, the network attempts to generate the neighboring stereo image by sampling pixels from the opposite image. Our image formation model uses the image sampler from the spatial transformer network (STN) [36] to sample the input image using a disparity map. The STN uses bilinear sampling where the output pixel is the weighted sum of four input pixels. In contrast to alternative approaches [9], [11], the bilinear sampler used is locally fully differentiable and integrates seamlessly into our fully convolutional architecture. This means that we do not require any simplification or approximation of our cost function.

Inspired by [38], for  $N$  pixels we use a combination of an  $L1$  and single scale SSIM [39] term as our photometric, image reconstruction, cost  $C_{ap}$ , between the input image  $I_{ij}^l$  and its reconstruction  $\tilde{I}_{ij}^l$ ,

$$C_{ap}^l = \frac{1}{N} \sum_{i,j} \alpha \frac{1 - \text{SSIM}(I_{ij}^l, \tilde{I}_{ij}^l)}{2} + (1-\alpha) \|I_{ij}^l - \tilde{I}_{ij}^l\|. \quad (3)$$

Here, we use a simplified SSIM with a  $3 \times 3$  block filter instead of a Gaussian, and set  $\alpha = 0.85$ .

### Disparity Smoothness Loss

We encourage disparities to be locally smooth with an  $L1$  penalty on the disparity gradients  $\partial d$ . As depth discontinuities often occur at image gradients, similar to [40], we weight this cost with an edge aware term using the corresponding image gradients  $\partial I$ ,

$$C_{ds}^l = \frac{1}{N} \sum_{i,j} |\partial_x d_{ij}^l| e^{-\eta \|\partial_x I_{ij}^l\|} + |\partial_y d_{ij}^l| e^{-\eta \|\partial_y I_{ij}^l\|}, \quad (4)$$

where we set  $\eta = 1.0$  in all our experiments.

### Left-Right Disparity Consistency Loss

To produce more robust results, we train our network to predict both the left and right image disparities, while only being given the left view as input to the convolutional part of the network. To ensure coherence, we introduce an  $L1$  left-right disparity consistency penalty as part of our model. This cost attempts to make the left-view disparity map be equal to the projected right-view disparity map,

$$C_{lr}^l = \frac{1}{N} \sum_{i,j} |d_{ij}^l - d_{ij+d_{ij}^l}^r|. \quad (5)$$

Like all the other terms, this cost is mirrored for the right-view disparity map and is evaluated at all of the output scales.

TABLE 1

Our network architecture, where  $k$  is the kernel size,  $s$  the stride, **channels** the number of input and output channels of each layer, **in** and **out** the input and output downscaling factor for each layer relative to the input image, and **input** corresponds to the input of each layer where  $+$  means concatenation and  $*$  corresponds to a  $2 \times$  upsampling of the corresponding layer.

layer	k	s	channels	in	out	input
conv1	7	2	3/32	1	2	left
conv1b	7	1	32/32	2	2	conv1
conv2	5	2	32/64	2	4	conv1b
conv2b	5	1	64/64	4	4	conv2
conv3	3	2	64/128	4	8	conv2b
conv3b	3	1	128/128	8	8	conv3
conv4	3	2	128/256	8	16	conv3b
conv4b	3	1	256/256	16	16	conv4
conv5	3	2	256/512	16	32	conv4b
conv5b	3	1	512/512	32	32	conv5
conv6	3	2	512/512	32	64	conv5b
conv6b	3	1	512/512	64	64	conv6
conv7	3	2	512/512	64	128	conv6b
conv7b	3	1	512/512	128	128	conv7
upconv7	3	2	512/512	128	64	conv7b
iconv7	3	1	1024/512	64	64	upconv7+conv6
upconv6	3	2	512/512	64	32	iconv7
iconv6	3	1	1024/512	32	32	upconv6+conv5
upconv5	3	2	512/256	32	16	iconv6
iconv5	3	1	512/256	16	16	upconv5+conv4
upconv4	3	2	256/128	16	8	iconv5
iconv4	3	1	128/128	8	8	upconv4+conv3
disp4	3	1	128/2	8	8	iconv4
upconv3	3	2	128/64	8	4	iconv4
iconv3	3	1	66/64	4	4	upconv3+conv2+disp4*
disp3	3	1	64/2	4	4	iconv3
upconv2	3	2	64/32	4	2	iconv3
iconv2	3	1	34/32	2	2	upconv2+conv1+disp3*
disp2	3	1	32/2	2	2	iconv2
upconv1	3	2	32/16	2	1	iconv2
iconv1	3	1	18/16	1	1	upconv1+disp2*
disp1	3	1	16/2	1	1	iconv1

At test time, using a single forward pass through the network, the disparity at the finest scale level for the left image,  $d^l$ , is output as our prediction (this corresponds to  $displ$  from Table 1). As a result of the upsampling layers in our network, this prediction is the same resolution as the input image. Using the known camera baseline and focal length from the training set, we then convert from the disparity map to a depth map. While we also estimate the right disparity,  $d^r$ , during training, it is not used at test time.

## 4 RESULTS

Here we compare the performance of our approach to both supervised and unsupervised single view depth estimation methods. We train on rectified binocular stereo image pairs, and do not require any supervision in the form of ground truth depth. Existing single image datasets, such as [41], that lack stereo pairs, are not suitable for evaluation [41]. To evaluate our image formation model, we compare to a variant of our model that uses the Deep3D [9] image formation model, and a baseline that does not use the left-right consistency constraint.

### 4.1 Implementation Details

Our network architecture is outlined in Table 1 and consists of 31 million parameters that we learn. The network is implemented

in Torch [42] and takes on the order of 20 hours to train using 2 NVIDIA GeForce GTX TITAN X GPUs on a dataset of 30 thousand images for 50 epochs. Inference is fast and takes less than 50 ms (or more than 20 frames per second) for an  $768 \times 256$  image, including transfer times to and from the GPU.

During optimization, we set the weighting of the different loss components to  $\alpha_{ap} = 1$  and  $\alpha_{lr} = 1$ . The possible output disparities are constrained to be between 0 and  $d_{max}$  using a scaled sigmoid non-linearity, where  $d_{max} = 0.3 \times$  the image width at a given output scale. As a result of our multi-scale output, the typical disparity of neighboring pixels will differ by a factor of two between each scale (as we are upsampling the output by a factor of two). To correct for this, we scale the disparity smoothness term  $\alpha_{ds}$  with  $r$  for each scale, to get equivalent smoothing at each level. Thus  $\alpha_{ds} = 0.1/r$ , where  $r$  is the downscaling factor of the corresponding layer with respect to the resolution of the input image that is passed into the network (in from Table 1).

For the non-linearities in the network, we used exponential linear units [43] instead of the commonly used rectified liner units (ReLU) [44]. We found that ReLUs tended to prematurely fix the predicted disparities at intermediate scales to a single value, making subsequent improvement difficult. We trained our model from scratch for 50 epochs using Adam [45] where  $\beta_1 = 0.9$ ,  $\beta_2 = 0.999$ , and  $\epsilon = 10^{-8}$ . We used an initial learning rate of  $\lambda = 10^{-4}$  which we kept constant for the first 30 epochs before halving it every 10 epochs until the end. Initially, we experimented with progressive update schedules, as in [20], where lower resolution image scales were optimized first. However, we found that optimizing all four scales at once led to more stable convergence. Similarly, we use an identical weighting of each scale loss because we found that weighting them differently led to unstable convergence, hence we set  $\lambda_s = 1$  for all  $s$ . We experimented with batch normalization [46], but found that it did not produce a significant improvement, and ultimately excluded it.

Data augmentation was performed on the fly and it included horizontally flipping the input images and then swapping the left and right images so they were still in the correct position relative to each other. For color augmentations, we performed random gamma, brightness, and color shifts by sampling from uniform distributions in the ranges  $[0.8, 1.2]$  for gamma,  $[0.5, 2.0]$  for brightness, and  $[0.8, 1.2]$  for each color channel separately.

## 4.2 KITTI

We present results for the KITTI dataset [47] using two different test splits, to enable comparison to existing works. In its raw form, the dataset contains 42,382 images, with a typical image being  $1242 \times 375$  pixels in size. As no official test split exists for the raw data, to ensure no overlap between the training set and the test images we remove frames that are within  $\pm 5$  frames of a given test image. As the car capturing the data is usually moving while capturing images at 10 frames per second, this strategy reduces the overlap between the two splits.

### 4.2.1 KITTI Split

First we compare different variants of our method including different image formation models and different training sets. We evaluate on the 200 high quality disparity images provided as part of the official KITTI training set. While these disparity images are much better quality than the reprojected velodyne laser

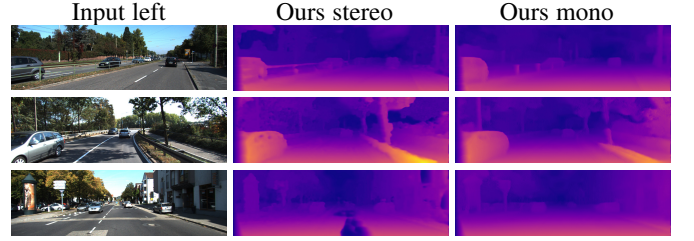


Fig. 4. Our stereo results. The disparity maps are sharper and more accurate than the single image case but, as seen in the last row, they can sometimes exhibit artifacts in low textured regions such as the hole seen here in the road.

depth values, they have CAD models inserted in place of moving cars. Such model-fitting results in ambiguous disparity values on transparent regions such as car windows, and issues at object boundaries where the CAD models do not perfectly align with the images. Our evaluation is performed on the full input image resolution, and the total number of training images is 40,046. In addition, the maximum depth present in the KITTI dataset is on the order of 80 meters, and we cap the maximum predictions of all networks to this value. Results are computed using the depth metrics from [2] along with the *D1-all* disparity error from KITTI [47]. It is important to note that measuring the error in depth space while the ground truth is given in disparities leads to precision issues. The metrics from [2] measure error in both meters from the ground truth and the percentage of depths that are within some threshold from the correct value. In particular, the non-thresholded measures can be sensitive to the large errors in depth caused by prediction errors at small disparity values.

In Table 2, we see that in addition to having poor scaling properties (in terms of both resolution and the number of disparities it can represent), when trained from scratch and given the same network architecture as ours, the Deep3D [9] image formation model performs poorly. From Fig. 3 we can see that Deep3D produces plausible image reconstructions but the output disparities are inferior to ours. Our loss outperforms the Deep3D baseline and the addition of the left-right consistency check increases performance in all measures. In Fig. 5 we illustrate some zoomed in comparisons, clearly showing that the inclusion of the left-right check improves the visual quality of the results. Our results are further improved by first pretraining our model with additional training data from the Cityscapes dataset [48] containing 22,973 training stereo pairs captured in various cities across Germany. This dataset brings higher resolution, image quality, and variety compared to KITTI, while having a similar setting. We cropped the input images to only keep the top 80 % of the image, to remove the very reflective car hoods from the input. Interestingly, our model trained on Cityscapes alone does not perform very well numerically. This is likely due to the difference in camera calibration between the two datasets, but there is a clear advantage to finetuning on data that is related to the test set.

### 4.2.2 Eigen Split

To be able to compare to existing work, we also use the test split of 697 images as proposed by [2] which results in 33,131 images for training. To generate the ground truth depth images, we reproject the 3D points viewed from the velodyne laser into the left input color camera. Aside from only producing depth values for less than 5% of the pixels in the input image, errors are also introduced because of the rotation of the Velodyne, the

TABLE 2

Comparison of different image formation models. Results on the KITTI 2015 stereo dataset [47] using the official 200 training set test images. For training, K is the KITTI dataset [47] and CS is Cityscapes [48]. Our model with the left-right consistency performs the best. Additionally, we can benefit by using more training data from the Cityscapes dataset. The last row shows the result of our model trained and tested with two input images instead of one.

Method	Dataset	Resolution	Abs Rel	Sq Rel	RMSE	RMSE log	<i>DI-all</i>	$\delta < 1.25$	$\delta < 1.25^2$	$\delta < 1.25^3$
Ours with Deep3D [9] mean	K	128 × 384	0.250	3.236	9.274	0.432	60.624	0.626	0.810	0.894
Ours with Deep3D [9] argmax	K	128 × 384	0.412	16.374	13.693	0.512	66.850	0.690	0.833	0.891
Ours without LR	K	256 × 768	0.110	1.774	5.617	0.188	20.875	0.896	0.962	0.982
Ours	K	256 × 768	0.098	<b>1.218</b>	5.265	<b>0.175</b>	19.485	0.899	0.964	0.984
Ours	CS	256 × 512	0.651	9.128	13.770	0.516	93.900	0.064	0.431	0.890
Ours	CS + K	256 × 512	<b>0.097</b>	1.265	<b>5.243</b>	<b>0.175</b>	<b>18.546</b>	<b>0.904</b>	<b>0.966</b>	<b>0.985</b>
Ours Stereo	K	256 × 768	0.118	3.155	5.746	0.197	10.580	0.931	0.967	0.980
Lower is better							Higher is better			

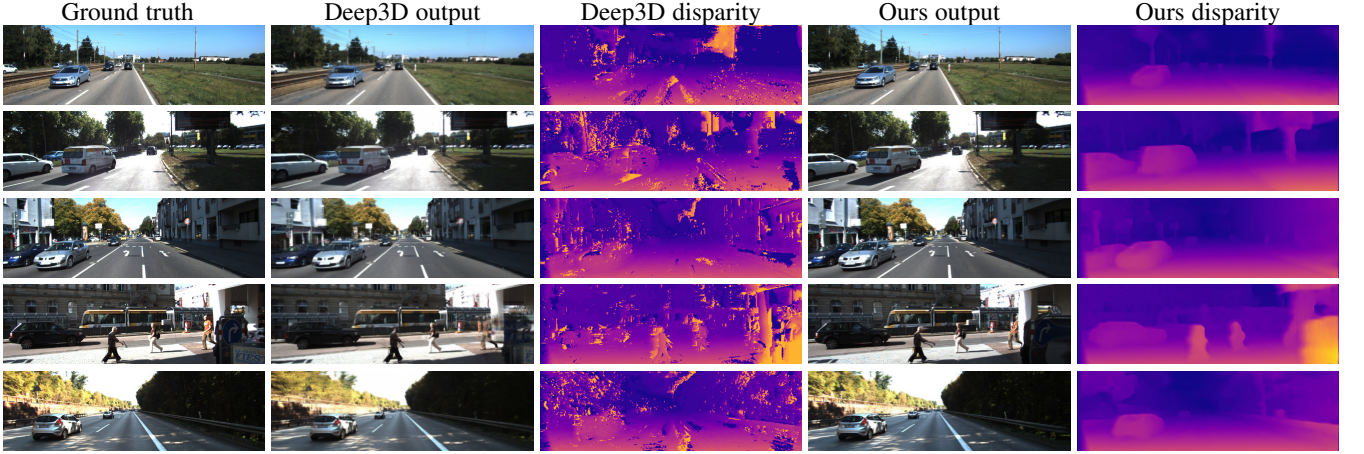


Fig. 3. Both the Deep3D image formation model and our approach produce plausible image reconstructions for the right view. However the disparities produced by Deep3D are noisier than ours. The Deep3D disparity maps are obtained by assigning each pixel to the disparity with the highest probability.

motion of the vehicle and surrounding objects, and also incorrect readings due to occlusion at object boundaries. To be fair to all methods, we use the same crop as [2] and evaluate at the input image resolution. With the exception of Garg et al.'s [11] results, the results of the baseline methods are recomputed by us given the authors's original predictions to ensure that all the scores are directly comparable. This produces slightly different numbers than the previously published ones, e.g. in the case of [2], their predictions were evaluated on much smaller depth images (1/4 the original size). For all methods we use bilinear interpolation to resize the predictions to the correct input image size.

Quantitative results are presented in Table 3 with some example outputs shown in Fig. 6. We see that our algorithm outperforms all other existing methods, including those that are trained with ground truth depth images. We again see that pretraining on the Cityscapes dataset improves the results over using KITTI alone.

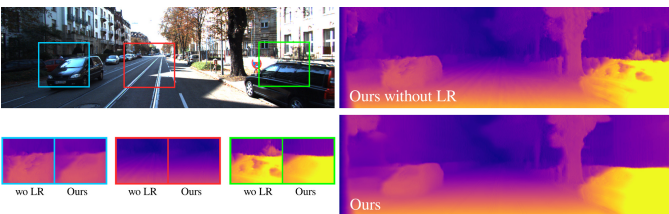


Fig. 5. Comparison between our method with and without the left-right consistency. Our consistency term produces superior results on the object boundaries.

### 4.3 Stereo

We also implemented a stereo version of our architecture, where instead of only feeding the left image to the network, we use both left and right views. While the depth errors in Table 2 are worse for some of the error measures than in the single image case, the stereo model performs significantly better on the *DI-all* disparity measure. The higher errors of the stereo model on the distance based metrics can be explained by its tendency to incorrectly estimate the depths of texture-less regions of the road, as can be seen in Fig. 4.

### 4.4 Make3D

To illustrate that our method can generalize to other datasets, here we compare to several fully supervised methods on the Make3D test set of [24]. We use our network trained only on the Cityscapes dataset and despite the dissimilarities in the datasets, both in content and camera parameters, we still achieve reasonable results. Due to the different aspect ratio of the Make3D dataset we evaluated on a central crop of the images. We use the same crop of their full frame results when evaluating the baseline methods. In Table 4, we compare our output to the similarly cropped results of the other methods. As in the case of the KITTI dataset, these results would likely be improved with more relevant training data. A qualitative comparison to some of the related methods is shown in Fig. 7. While our numerical results are worse than the baselines, qualitatively, we compare favorably to the supervised competition.

TABLE 3

Results on the KITTI 2015 stereo dataset [47] using the split of Eigen et al. [2]. For training, K is the KITTI dataset [47] and CS is Cityscapes [48].

The predictions provided by Liu et al. [3]\* are generated on a mix of the left and right images instead of just the left input images. For a fair comparison, we recompute their results using the corresponding right or left image. Eigen et al. [2]° compute distance to the velodyne instead of the camera. For fairness, we also compute their results relative to the velodyne. The results from Garg et al. [11] are taken directly from their paper. Again for fair comparison, we use the same crop and maximum evaluation distance as them.

Method	Supervised	Dataset	Abs Rel	Sq Rel	RMSE	RMSE log	$\delta < 1.25$	$\delta < 1.25^2$	$\delta < 1.25^3$
Train set mean	No	K	0.403	5.530	8.709	0.403	0.593	0.776	0.878
Eigen et al. [2] Coarse °	Yes	K	0.206	1.531	6.414	0.269	0.689	0.891	0.960
Eigen et al. [2] Fine °	Yes	K	0.197	1.485	6.179	0.260	0.712	0.895	0.961
Liu et al. [3] DCNF-FCSP FT *	Yes	K	0.217	1.841	6.986	0.289	0.647	0.882	0.961
<b>Ours without LR</b>	No	K	0.150	2.062	6.220	0.252	0.819	0.928	0.964
<b>Ours</b>	No	K	0.141	<b>1.369</b>	5.849	0.242	0.818	0.929	0.966
<b>Ours</b>	No	CS + K	<b>0.136</b>	1.512	<b>5.763</b>	<b>0.236</b>	<b>0.836</b>	<b>0.935</b>	<b>0.968</b>
Garg et al. [11] L12 Aug 8× cap 50m	No	K	0.169	1.080	5.104	0.273	0.740	0.904	0.962
<b>Ours cap 50m</b>	No	K	0.123	0.944	5.061	0.221	0.843	0.942	0.972
<b>Ours cap 50m</b>	No	CS + K	<b>0.118</b>	<b>0.932</b>	<b>4.941</b>	<b>0.215</b>	<b>0.858</b>	<b>0.947</b>	<b>0.974</b>

Lower is better

Higher is better

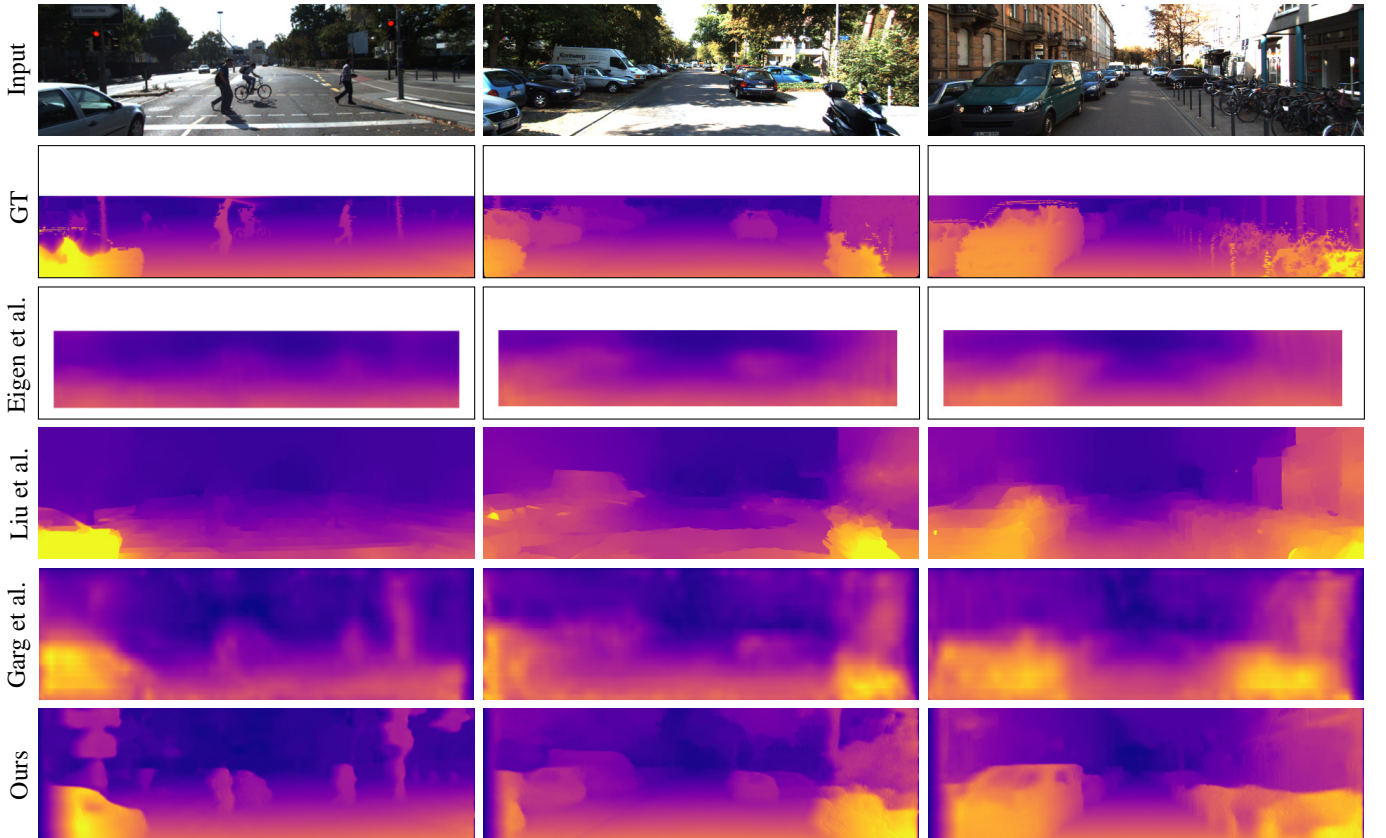


Fig. 6. Qualitative results on the KITTI Eigen Split. The ground truth computed from the velodyne is very spare, here we interpolate it for visualization purposes. Our method does better at resolving small objects such as the pedestrians and poles.

TABLE 4

Results on the Make3D dataset [24]. All methods marked with \* use ground truth depth data from the Make3D training set to build their model. Using the standard C1 metric, errors are only computed where depth is less than 70 meters in a central image crop.

Method	Abs Rel	RMSE	RMSE log
Train set mean*	0.900	11.59	0.224
Karsch et al. [26]*	0.411	8.159	0.144
Liu et al. [49]*	0.450	10.11	0.159
Laina et al. [30] berHu*	<b>0.197</b>	<b>5.472</b>	<b>0.082</b>
<b>Ours w/ Deep3D [9] argmax</b>	1.000	18.40	2.527
<b>Ours</b>	0.552	11.58	0.165

#### 4.5 Generalizing to Other Datasets

Finally, we illustrate some further examples of our model generalizing to other datasets. Using the model only trained on Cityscapes [48], we tested on the CamVid driving dataset [50]. In Fig. 8 we can see that despite the differences in location, image characteristics, and camera calibration, our model still produces visually plausible depths. We also captured a 20,000 frame dataset by extracting 5 images per second from a pair of videos taken with two synchronized consumer cameras with 30 mm lenses. Finetuning the Cityscapes pretrained model on this dataset produces visually convincing depth images for a test set that was captured with the same rig on a different day, see Fig. 8

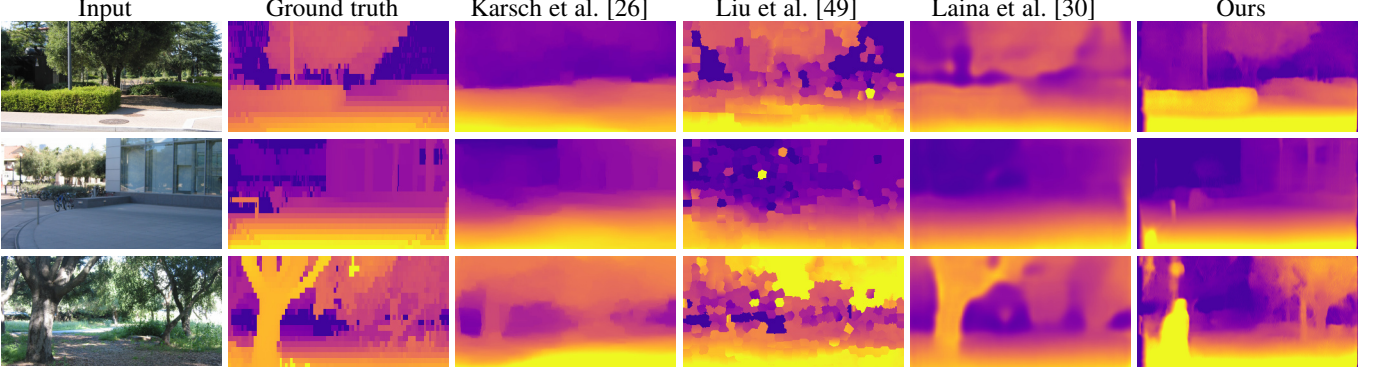


Fig. 7. Our method achieves good qualitative results on Make3D despite being trained on a different dataset. A failure case is visible in the last row where our method is confused by the shadow and seems to synthesize depth for a human instead of a tree.

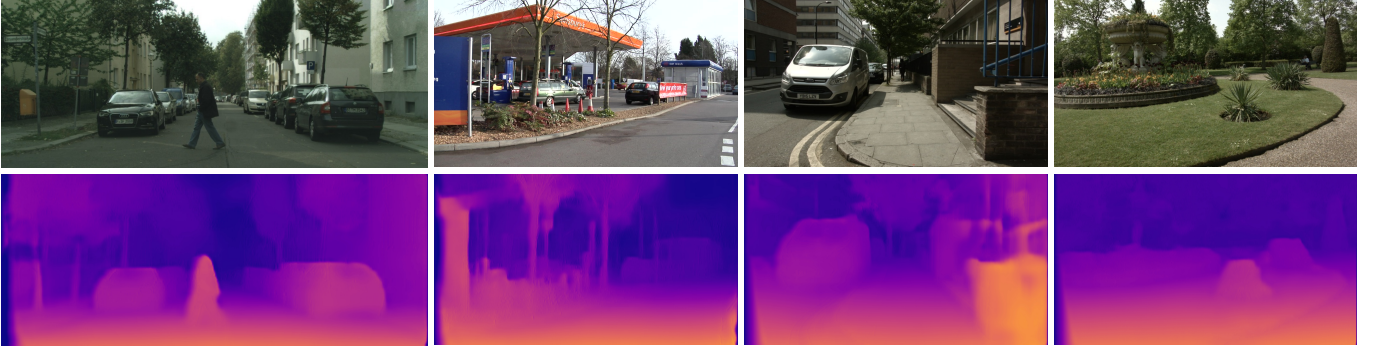


Fig. 8. Qualitative results for our model, trained on Cityscapes, generalizing to the Cityscapes test set [48], CamVid [50], and two test scenes from our own dataset of handheld urban videos.

and the video on our project website<sup>1</sup>.

#### 4.6 Limitations

Even though our left-right consistency check improves the quality of the results, there are still some artifacts visible at occlusion boundaries due to the pixels in the occlusion region not being visible in both images. Issues due to occlusion are also apparent at the left image border where the corresponding pixels are also typically not visible in the second view. It may be possible to improve some of these issues by more explicitly reasoning about occlusion during training [51], [52]. It is worth noting that depending how large the baseline between the camera and the depth sensor, fully supervised approaches also do not always have valid depth for all pixels.

While our method only needs a single image at test time to predict a scene’s depth, it does require rectified and temporally aligned stereo pairs during training. This means that it is currently not possible to use existing single-view datasets for training purposes e.g. [41]. However, it is possible to fine-tune our model on application specific ground truth depth data. Our image reconstruction term is computed in pixel space, where the brightness constancy assumption is violated on specular [53] and transparent surfaces. This could be improved with alternative similarity measures [17].

## 5 CONCLUSION

We have presented an unsupervised deep neural network for single image depth estimation. Instead of using aligned ground truth

depth data, which is both rare and costly, we exploit the ease with which binocular stereo data can be captured. Our novel loss function enforces consistency between the predicted depth maps from each camera view during training, leading to improved predictions. Our results are superior to fully supervised baselines, which is encouraging for future research that does not require expensive to capture ground truth depth. We have also shown that our model can generalize to datasets not seen during training and still produce visually plausible depth maps.

In future work, we would like to extend our model to videos. Our current depth estimates are performed independently per frame, but it could be useful if they were temporally consistent [26]. It would also be interesting to investigate sparse input as an alternative training signal [54], [55]. Finally, while our model estimates per pixel depth, for many applications it would be useful to also predict the full occupancy for both visible and occluded regions [56].

**Acknowledgments** We would like to thank Fayao Liu, David Eigen, Iro Laina, and Ravi Garg for provided data and code to recreate the baseline algorithms. We also thank Stephan Garbin for his invaluable help throughout this project.

## REFERENCES

- [1] L. Ladicky, J. Shi, and M. Pollefeys, “Pulling things out of perspective,” in *CVPR*, 2014.
- [2] D. Eigen, C. Puhrsch, and R. Fergus, “Depth map prediction from a single image using a multi-scale deep network,” in *NIPS*, 2014.
- [3] F. Liu, C. Shen, G. Lin, and I. Reid, “Learning depth from single monocular images using deep convolutional neural fields,” *PAMI*, 2015.

1. <http://visual.cs.ucl.ac.uk/pubs/monoDepth>

- [4] K. Karsch, K. Sunkavalli, S. Hadap, N. Carr, H. Jin, R. Fonte, M. Sittig, and D. Forsyth, “Automatic scene inference for 3d object compositing,” *TOG*, 2014.
- [5] J. T. Barron, A. Adams, Y. Shih, and C. Hernández, “Fast bilateral-space stereo for synthetic defocus,” *CVPR*, 2015.
- [6] I. Lenz, H. Lee, and A. Saxena, “Deep learning for detecting robotic grasps,” *The International Journal of Robotics Research*, 2015.
- [7] J. Shotton, T. Sharp, A. Kipman, A. Fitzgibbon, M. Finocchio, A. Blake, M. Cook, and R. Moore, “Real-time human pose recognition in parts from single depth images,” *Communications of the ACM*, 2013.
- [8] D. Stoyanov, M. V. Scarzanella, P. Pratt, and G.-Z. Yang, “Real-time stereo reconstruction in robotically assisted minimally invasive surgery,” in *MICCAI*, 2010.
- [9] J. Xie, R. Girshick, and A. Farhadi, “Deep3d: Fully automatic 2d-to-3d video conversion with deep convolutional neural networks,” in *ECCV*, 2016.
- [10] I. P. Howard, *Perceiving in depth, volume 1: basic mechanisms*. Oxford University Press, 2012.
- [11] R. Garg, V. Kumar BG, and I. Reid, “Unsupervised CNN for single view depth estimation: Geometry to the rescue,” in *ECCV*, 2016.
- [12] D. Scharstein and R. Szeliski, “A taxonomy and evaluation of dense two-frame stereo correspondence algorithms,” *IJCV*, 2002.
- [13] Y. Furukawa and C. Hernández, “Multi-view stereo: A tutorial,” *Foundations and Trends in Computer Graphics and Vision*, 2015.
- [14] R. Ranftl, V. Vineet, Q. Chen, and V. Koltun, “Dense monocular depth estimation in complex dynamic scenes,” in *CVPR*, 2016.
- [15] R. J. Woodham, “Photometric method for determining surface orientation from multiple images,” *Optical engineering*, 1980.
- [16] A. Abrams, C. Hawley, and R. Pless, “Heliometric stereo: Shape from sun position,” in *ECCV*, 2012.
- [17] J. Žbontar and Y. LeCun, “Stereo matching by training a convolutional neural network to compare image patches,” *JMLR*, 2016.
- [18] L. Ladicky, C. Häne, and M. Pollefeys, “Learning the matching function,” *arXiv preprint arXiv:1502.00652*, 2015.
- [19] W. Luo, A. Schwing, and R. Urtasun, “Efficient deep learning for stereo matching,” in *CVPR*, 2016.
- [20] N. Mayer, E. Ilg, P. Häusser, P. Fischer, D. Cremers, A. Dosovitskiy, and T. Brox, “A large dataset to train convolutional networks for disparity, optical flow, and scene flow estimation,” in *CVPR*, 2016.
- [21] E. Shelhamer, J. Long, and T. Darrell, “Fully convolutional networks for semantic segmentation,” *PAMI*, 2016.
- [22] P. Fischer, A. Dosovitskiy, E. Ilg, P. Häusser, C. Hazirbas, V. Golkov, P. van der Smagt, D. Cremers, and T. Brox, “Flownet: Learning optical flow with convolutional networks,” in *ICCV*, 2015.
- [23] A. Gaidon, Q. Wang, Y. Cabon, and E. Vig, “Virtual worlds as proxy for multi-object tracking analysis,” in *CVPR*, 2016.
- [24] A. Saxena, M. Sun, and A. Y. Ng, “Make3d: Learning 3d scene structure from a single still image,” *PAMI*, 2009.
- [25] D. Hoiem, A. A. Efros, and M. Hebert, “Automatic photo pop-up,” *TOG*, 2005.
- [26] K. Karsch, C. Liu, and S. B. Kang, “Depth transfer: Depth extraction from video using non-parametric sampling,” *PAMI*, 2014.
- [27] D. Eigen and R. Fergus, “Predicting depth, surface normals and semantic labels with a common multi-scale convolutional architecture,” in *ICCV*, 2015.
- [28] B. Li, C. Shen, Y. Dai, A. van den Hengel, and M. He, “Depth and surface normal estimation from monocular images using regression on deep features and hierarchical crfs,” in *CVPR*, 2015.
- [29] Y. Cao, Z. Wu, and C. Shen, “Estimating depth from monocular images as classification using deep fully convolutional residual networks,” *arXiv preprint arXiv:1605.02305*, 2016.
- [30] I. Laina, C. Rupprecht, V. Belagiannis, F. Tombari, and N. Navab, “Deeper depth prediction with fully convolutional residual networks,” *arXiv preprint arXiv:1606.00373*, 2016.
- [31] X. Wang, D. Fouhey, and A. Gupta, “Designing deep networks for surface normal estimation,” in *CVPR*, 2015.
- [32] J. Flynn, I. Neulander, J. Philbin, and N. Snavely, “Deepstereo: Learning to predict new views from the world’s imagery,” in *CVPR*, 2016.
- [33] V. Patraucean, A. Handa, and R. Cipolla, “Spatio-temporal video autoencoder with differentiable memory,” *arXiv preprint arXiv:1511.06309*, 2015.
- [34] T. Zhou, P. Krähenbühl, M. Aubry, Q. Huang, and A. A. Efros, “Learning dense correspondence via 3d-guided cycle consistency,” *CVPR*, 2016.
- [35] T. Zhou, S. Tulsiani, W. Sun, J. Malik, and A. A. Efros, “View synthesis by appearance flow,” in *ECCV*, 2016.
- [36] M. Jaderberg, K. Simonyan, A. Zisserman, and K. Kavukcuoglu, “Spatial transformer networks,” in *NIPS*, 2015.
- [37] R. Hartley and A. Zisserman, *Multiple view geometry in computer vision*. Cambridge university press, 2003.
- [38] H. Zhao, O. Gallo, I. Frosio, and J. Kautz, “Is l2 a good loss function for neural networks for image processing?” *arXiv preprint arXiv:1511.08861*, 2015.
- [39] Z. Wang, A. C. Bovik, H. R. Sheikh, and E. P. Simoncelli, “Image quality assessment: from error visibility to structural similarity,” *Transactions on Image Processing*, 2004.
- [40] P. Heise, S. Klose, B. Jensen, and A. Knoll, “Pm-huber: Patchmatch with huber regularization for stereo matching,” in *ICCV*, 2013.
- [41] P. K. Nathan Silberman, Derek Hoiem and R. Fergus, “Indoor segmentation and support inference from rgbd images,” in *ECCV*, 2012.
- [42] R. Collobert, K. Kavukcuoglu, and C. Farabet, “Torch7: A matlab-like environment for machine learning,” in *BigLearn, NIPS Workshop*, 2011.
- [43] D.-A. Clevert, T. Unterthiner, and S. Hochreiter, “Fast and accurate deep network learning by exponential linear units (elus),” *arXiv preprint arXiv:1511.07289*, 2015.
- [44] V. Nair and G. E. Hinton, “Rectified linear units improve restricted boltzmann machines,” in *ICML*, 2010.
- [45] D. Kingma and J. Ba, “Adam: A method for stochastic optimization,” *arXiv preprint arXiv:1412.6980*, 2014.
- [46] S. Ioffe and C. Szegedy, “Batch normalization: Accelerating deep network training by reducing internal covariate shift,” *arXiv preprint arXiv:1502.03167*, 2015.
- [47] A. Geiger, P. Lenz, and R. Urtasun, “Are we ready for autonomous driving? the kitti vision benchmark suite,” in *CVPR*, 2012.
- [48] M. Cordts, M. Omran, S. Ramos, T. Rehfeld, M. Enzweiler, R. Benenson, U. Franke, S. Roth, and B. Schiele, “The cityscapes dataset for semantic urban scene understanding,” in *CVPR*, 2016.
- [49] M. Liu, M. Salzmann, and X. He, “Discrete-continuous depth estimation from a single image,” in *CVPR*, 2014.
- [50] G. J. Brostow, J. Fauqueur, and R. Cipolla, “Semantic object classes in video: A high-definition ground truth database,” *Pattern Recognition Letters*, 2009.
- [51] D. Hoiem, A. N. Stein, A. A. Efros, and M. Hebert, “Recovering occlusion boundaries from a single image,” in *ICCV*, 2007.
- [52] A. Humayun, O. Mac Aodha, and G. J. Brostow, “Learning to Find Occlusion Regions,” in *CVPR*, 2011.
- [53] C. Godard, P. Hedman, W. Li, and G. J. Brostow, “Multi-view reconstruction of highly specular surfaces in uncontrolled environments,” in *3DV*, 2015.
- [54] D. Zoran, P. Isola, D. Krishnan, and W. T. Freeman, “Learning ordinal relationships for mid-level vision,” in *ICCV*, 2015.
- [55] W. Chen, Z. Fu, D. Yang, and J. Deng, “Single-image depth perception in the wild,” in *NIPS*, 2016.
- [56] M. Firman, O. Mac Aodha, S. Julier, and G. J. Brostow, “Structured Prediction of Unobserved Voxels From a Single Depth Image,” in *CVPR*, 2016.